Ionospheric contribution to Saturn's inner plasmasphere

Luke Moore and Michael Mendillo
Center for Space Physics, Boston University, Boston, Massachusetts, USA

Received 2 November 2004; revised 26 January 2005; accepted 28 February 2005; published 24 May 2005.

[1] Ion densities from the three-dimensional Saturn thermosphere-ionosphere model are extended above the plasma exobase using the formalism of Pierrard and Lemaire (1996) which evaluates the balance of gravitational, centrifugal, and electric forces on plasma in a rotating dipole field. The parameter space of ionospheric contributions to Saturn's inner plasmasphere (to within 1 Saturnian radius above the limb, $L < 2$) is explored by comparing results that span the observed extremes of plasma temperature, 650–1700 K, and the range of velocity distribution functions, Lorentzian (or Kappa, with $\kappa = 2$) to Maxwellian (i.e., a Lorentzian with $\kappa = \infty$). Plasmaspheric densities are generated for solstice and equinox conditions using solar maximum and solar minimum solar fluxes. Magnetic flux tubes in Saturn's inner plasmasphere are modeled to have less plasma above the exobase ($\sim$4000 km) than below it in contrast to the terrestrial situation. Calculations are made for plasma densities along the path of the Cassini spacecraft's orbital insertion on 1 July 2004. The full range of modeled electron density at closest approach is 0.02–220 cm^{-3}, although increased knowledge of either plasma temperature or velocity distribution at Saturn's plasma exobase would tighten this range considerably. There is reason to favor the higher values of the calculated electron density as the plasma population at Saturn's plasma exobase is more likely to exhibit a non-Maxwellian velocity distribution. There is a wide range of combinations of κ and plasma temperature that leads to predictions of order 100 el cm^{-3} at Cassini's closest approach, 1.3 R_S.

Citation: Moore, L., and M. Mendillo (2005), Ionospheric contribution to Saturn's inner plasmasphere, *J. Geophys. Res.*, *110*, A05310, doi:10.1029/2004JA010889.

1. Introduction

1.1. Definition of a Plasmasphere

[2] The term plasmasphere was introduced in the 1960s to describe the region of low-energy ions and electrons between the inner "terrestrial spheres" of ionosphere/exosphere and the large-scale magnetosphere created by solar wind flow past the magnetized planet. The dipole field is strong in the inner magnetosphere ($L < \sim 4\ R_E$), where L is distance in units of Earth radii (R_E), and the diurnal rotation of the planet results in nearly corotating dipole flux tubes and the plasma they contain. The magnetospheric convection patterns induced by the solar wind interaction can have velocities comparable to corotation near $L = 5–6$. Solar wind variability causes these two flow patterns to interact continuously, creating a dynamically evolving region of plasma that encircles Earth in the 3–6 R_E domain, separated by a local time-dependent plasmapause from the vast regions of sunward convection beyond.

[3] The ionization within the plasmasphere is composed overwhelmingly of low-energy ions and electrons that have diffused upward from the ionosphere. The coupling is not, however, a simple one-way (i.e., upward) process. On a diurnal basis, there is a significant interchange of plasma between the F2 region of the ionosphere (traditionally assigned its "top" at 1000 km altitude) and the plasmasphere above. These fluxes involve a change in ionic mass in the topside ionosphere as photochemically produced O^+ ions interact with hydrogen gas and vice versa, resulting in the domain above the ionosphere being originally designated the "protonosphere." The downward flux is typically $\sim 10^8$ el cm^{-2} s^{-1}, a value crucial to the maintenance of the nighttime ionosphere from a more complete chemical decay after sunset. The upward flux returns ionization to the plasmaspheric tubes during the daytime, and thus a plasmaspheric content variation of 20–30% occurs on a daily basis. Comprehensive summaries of plasmaspheric science are given by *Carpenter and Park* [1973] and more recently by *Burch* [2003].

[4] Saturn's plasmasphere is quite different from Earth's because of the presence of an extraordinary ring system and the moon Enceladus. These are nonatmospheric sources of neutrals (and therefore plasmas) sputtered from the rings and moon that can add plasma to flux tubes in rotation around Saturn. The rings can also absorb (i.e., neutralize) plasma that reaches the equatorial plane at ring locations, and thus rings can be both a source and a loss mechanism. The rings and Enceladus were not thought to be as strong a source of gas and plasma as Io is at Jupiter, which

0148-0227/05/2004JA010889$09.00

presents yet another unique plasmaspheric regime. Modeling studies for Io have long used total source rates of $\sim 10^{28}$ neutral s^{-1} [*Dessler*, 1980; *Brown*, 1994], while at Saturn the most recent modeling studies suggest a comparable total rate, with 80% coming from the ~ 4 R_S domain encompassing Enceladus and Saturn's E ring (S. Jurac and J. D. Richardson, A self-consistent model of plasma and neutrals at Saturn: Neutral cloud morphology, submitted to *Journal of Geophysical Research,* 2004). Thus the plasma populations in Saturn's middle and outer magnetosphere are likely dominated by these internal sources of neutrals; however, the conclusions for the inner plasmasphere are not so clear. As demonstrated by *Nagy et al.* [1986] for Jupiter using a model similar to the one described in this study, there may be a significant cold plasma population in Saturn's plasmasphere that has an ionospheric origin.

[5] As the Cassini spacecraft begins to explore all of these processes in some detail, it is useful to continue with estimates of plasmaspheric sources via modeling. This paper addresses the purely ionospheric contribution to the inner magnetosphere ($L < 2$), i.e., a numerical study of the "classic plasmasphere" that might result from the distribution of upwardly diffusing ion-electron pairs from Saturn's topside ionosphere, as portrayed by the most recent model of Saturn's ionosphere.

1.2. Prior Work: Terrestrial and Giant Plasmaspheres

[6] Collisions between neutral particles within a planetary atmosphere produce bulk motions within the gas, causing it to exhibit fluid-like behavior. As the gas density decreases with height, the frequency of collisions also decreases with height, and thus there must be a region where collisions become so infrequent that they can be neglected altogether. The ideal transition boundary between a collisionally dominated barosphere below and a collisionless exosphere above is defined as the exobase. Typically, the critical level of this transition is chosen to be the height at which the mean free path of a particle is equal to the scale height of the atmosphere [*Spitzer*, 1949].

[7] In analogy to the neutral exobase, plasmaspheric models define the plasma exobase as the altitude where the mean free path of thermal ions, l, becomes larger than the scale height of the plasma, H_P [e.g., *Lemaire*, 1976]. Above the plasma exobase it is assumed that charged particles move without collisions along trajectories determined by their energy and pitch angle. This critical level will tend to be higher in altitude than that of the neutral constituents, as the Coulomb cross section is much larger than the gas-kinetic cross section for collision.

[8] As discussed by *Pierrard and Lemaire* [1996], *Lemaire and Scherer* [1974], and *Hartle* [1969, 1971], it is possible to derive plasma parameters along a flux tube with some knowledge (or assumption) of plasma parameters at the exobase. The velocity distribution function (VDF) at the exobase can be calculated at any other point in the exosphere from Liouville's theorem. Analytical expressions for other parameters of the plasma (e.g., density, flux, and temperature) can then be derived by taking moments of the VDF, extending the exobase values throughout the exosphere.

[9] Typically, the adopted velocity distribution function has taken the form of a Maxwellian VDF, whether dealing with a neutral exosphere or an ion exosphere (e.g., *Kim and Son* [2000], *Wilson and Waite* [1989], and preceding references in this section). While one might expect thermal equilibrium deep within the barosphere, it may prove to be a misleading assumption when applied near or above the exobase, where collisions are becoming less and less frequent. More recently, there has been much discussion in the literature favoring Lorentzian VDFs for space plasmas, which are generally observed to possess a non-Maxwellian high-energy tail [e.g., *Meyer-Vernet*, 2001].

[10] Regardless of velocity distribution, particles in a plasmasphere are constrained by the dipole magnetic field lines of the planet [*Angerami and Thomas*, 1964]. In a cold plasma limit with magnetic mirroring neglected one can derive an imaginary surface at which the field-aligned forces due to gravity and rotation are balanced. For Saturn the problem is simplified, as the rotational and magnetic axes are nearly coincident, in which case the radius of such a surface is given by

$$r_c = \left(\frac{2GM_S}{3\Omega^2} \sec^2 \lambda \right)^{\frac{1}{3}}, \tag{1}$$

where λ is latitude, $GM_S = 3.7925 \times 10^7$ km^3 s^{-2}, and $\Omega = 1.63778 \times 10^{-4}$ s^{-1} [*Ip*, 1983]. The extremely fast rotation of Saturn (10 hour 39.4 min period, a pre-Cassini value) leads to a critical radius of 1.6252 R_S at the equator. The net sum of field-aligned forces within the surface defined by equation (1) is directed downward, toward the ionosphere, while outside of the surface, forces are directed toward the equatorial plane. The fact that r_c is 1.6 R_S at the ring plane is interesting because this divides Saturn's rings into two regimes, with the inner half possibly siphoning plasma from the rings into the ionosphere [*Ip*, 1984a] and the plasma population of the outer half being susceptible to modifications by the rings [*Luhmann and Walker*, 1981].

[11] Ionospheric science at Saturn has been hampered by the sparse (and often controversial) data sets, providing little constraint for theoretical models. Specifically, to date, there are only five published electron density profiles from dawn/dusk radio occultations of the Pioneer (1979), Voyager 1 (1980), and Voyager 2 (1981) spacecraft, and they provide a wide range of peak electron densities, $0.6–2 \times 10^4$ cm^{-3}; peak heights, 1900–2900 km; and topside plasma scale heights, 250–1100 km [*Atreya et al.*, 1984]. Assuming, as *Moore et al.* [2004], *Moses and Bass* [2000], and *Majeed and McConnell* [1996] have calculated in their models, that H^+ is the dominant ion in Saturn's upper ionosphere, one can infer from the data topside plasma temperatures ranging from $\sim$260 to $\sim$1700 K. However, in an analysis of Voyager 2 EUV solar and stellar occultations, *Smith et al.* [1983] find a neutral exospheric temperature of 420 ± 30 K. Of the five occultations, only one inferred plasma temperature has the anomalous property of being smaller than the neutral exospheric temperature (the Voyager 2 egress). The range of the remaining plasma temperatures is $\sim$650–1700 K.

[12] This study extends previous ion exosphere studies of Saturn by making use of three-dimensional ion density profiles generated by the ionospheric model of *Moore et al.* [2004]. Ion densities given by Moore et al. are derived from a one-dimensional time-dependent ionospheric model

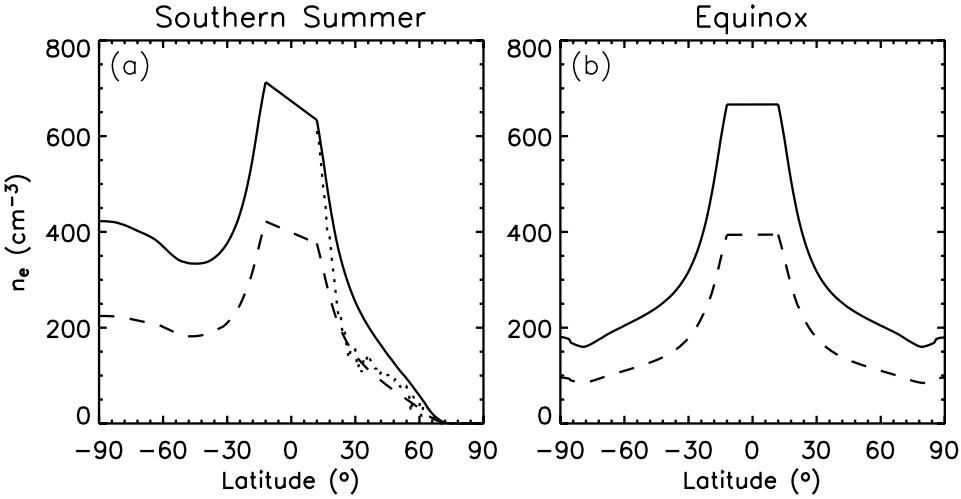

Figure 1. Distribution of ion densities at the plasma exobase calculated by the ionospheric module of Saturn thermosphere-ionosphere model during (a) southern summer and (b) equinox. Solid lines are for solar maximum, and dashed lines are for solar minimum. Figure 1a (dotted line) is for solar maximum calculations that include shadowing by Saturn's rings. Note that H^+ is the only ionospheric ion with significant density at these altitudes. At equatorial latitudes within 12° the electron densities do not relate to the region of Cassini's closest approach ($L \sim 1.3$); as equatorial electrodynamics are not yet included in the model, the equatorial densities have been truncated at their 50 day photochemical values.

that includes photochemistry and plasma diffusion and is coupled to a thermospheric global circulation model (GCM) described by I. C. F. Müller-Wodarg et al. (A global circulation model of Saturn's thermosphere, submitted to *Icarus*, 2005, hereinafter referred to as Müller-Wodarg et al., submitted manuscript, 2005). Thus exobase heights and densities are generated as a function of local time and latitude. Exobase ion compositions are extended into the plasmasphere using the collisionless formalism of *Pierrard and Lemaire* [1996]. As the model of Moore et al. does not yet calculate ion and electron temperatures self-consistently, results are obtained for plasma temperatures varying from 650 to 1700 K, the observed extremes from radio occultation profiles. Finally, calculations are made for plasmaspheric densities in the regions that the Cassini spacecraft will directly measure at Saturn.

2. Model

2.1. A Plasmasphere Component for the Saturn Thermosphere-Ionosphere Model

[13] *Moore et al.* [2004] and Müller-Wodarg et al. (submitted manuscript, 2005) represent the initial ionospheric and thermospheric results, respectively, from the Saturn thermosphere-ionosphere model (STIM), which is a classical GCM of Saturn's upper atmosphere. Previous studies of Saturn's plasmasphere have treated the exobase as a source constant in latitude and local time. The first global modeling results of Saturn's ionosphere reveal dramatic changes in ion densities as a function of latitude [*Moore et al.*, 2004], and thus STIM can advance plasmaspheric modeling at Saturn by providing a self-consistent, variable exobase. A brief outline of the STIM model is given below, after which the techniques for extending ionospheric densities into Saturn's exosphere are outlined.

[14] For realistic values of the solar irradiance, STIM incorporates the SOLAR2000 empirical model (currently version 2.25 [*Tobiska et al.*, 2000]). Representative solar maximum and solar minimum periods are used with $\langle$F10.7$\rangle$ of 180 and 70 units, respectively. After being attenuated by a model of the optical depth of Saturn's rings (for latitudes beneath the rings' shadow) these solar fluxes drive global structure within the thermospheric GCM and ionize the atmospheric constituents. Explicit time integration techniques are utilized to solve the Navier-Stokes equations of energy, momentum, and continuity (for the thermospheric GCM) and the ion continuity equations (for the ionospheric module). In the calculations shown here the model was run for 50 Saturn days, sufficient to achieve equilibrium at all latitudes except above the geomagnetic equator (see Figure 1).

[15] Saturn's observed exospheric neutral temperatures are not reproduced with solar EUV heating alone, a fact that holds true for other giant planets as well [*Gladstone et al.*, 2002; *Yelle and Miller*, 2004]. In order to model the observed temperatures, additional sources of heating are necessary. The STIM atmosphere for this study came from a representation of globally uniform wave heating from below as well as solar zenith angle–dependent solar heating from above (Müller-Wodarg et al., submitted manuscript, 2005). Auroral sources of heating and ionization are currently under investigation (C. G. A. Smith et al., Polar heating in Saturn's thermosphere, submitted to *Annales Geophysicae*, 2004; Müller-Wodarg et al., submitted manuscript, 2005); the assumption is made that the neglect of such effects upon thermospheric composition is not a primary concern for this study involving topside ionospheric densities at middle and low latitudes.

[16] To first order, models of Saturn's ionosphere show its peak electron density to be relatively constant with local

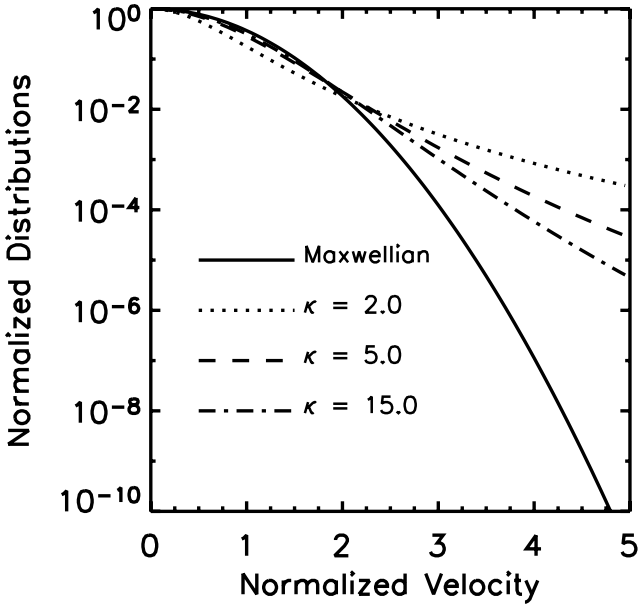

Figure 2. Comparison of a Maxwellian velocity distribution function (VDF) with three Lorentzian VDFs for κ = 2, 5, and 15.

time, calculating a diurnal variation of ~1.4 from midday electron density to midnight electron density [*Moore et al.*, 2004; *Majeed and McConnell*, 1996]. This minor variation vanishes higher up in the ionosphere, as H^+ ions become more dominant with increasing altitude. In this study, therefore, only latitudinal variations of the exobase are considered. Ion densities calculated by STIM during southern summer and equinox for minimum and maximum solar conditions are given in Figure 1. Note that considerable structure is apparent once ring shadowing is introduced into the model (Figure 1a, dotted line).

2.2. Plasmaspheric Model

[17] Ions and electrons in the plasmasphere will be distributed along magnetic field lines according to the balance of gravitational force with centrifugal force. These forces induce a charge separation electric field in the plasma. The combined potentials (gravitational, centrifugal, and electrostatic) help to define the equilibrium distribution of plasma emerging from the exobase. As described by *Lemaire* [1976], the number density along a magnetic field line above the exobase is determined by integrating the known (or assumed) VDF.

[18] The Maxwellian VDF is the most probable distribution of velocities for a gas in thermal equilibrium, i.e.,

$$f_M(v) = n\left(\frac{m}{2\pi k_B T}\right)^{\frac{3}{2}} \exp\left(-\frac{1}{2}mv^2/k_B T\right), \qquad (2)$$

where n is the plasma number density, m is the particle mass, k_B is Boltzmann's constant, T is the temperature, and v is the velocity. Thermal equilibrium seems an unlikely condition at the plasma exobase, however, which is located above the neutral exobase in altitude. Space plasmas have been shown observationally to possess non-Maxwellian high-energy tails [e.g., *Sittler et al.*, 1983; *Maksimovic et al.*, 1997]. In addition, *Hasegawa et al.* [1985] showed that a plasma immersed in superthermal radiation would assume a Lorentzian-like equilibrium distribution. The generalized Maxwellian VDF, often called the Lorentzian or Kappa distribution, is given as

$$f_L(v) = n\left[\frac{\kappa}{(2\kappa-3)}\frac{m}{\pi k_B T}\right]^{\frac{3}{2}} \frac{\Gamma(\kappa+1)}{\kappa^{\frac{3}{2}}\Gamma\left(\kappa-\frac{1}{2}\right)}\left[1+\frac{\kappa}{(2\kappa-3)}\frac{mv^2}{k_B T}\right]^{-(\kappa+1)}, \qquad (3)$$

where κ is the spectral index ($\kappa > 1.5$) and Γ is the gamma function. The Lorentzian VDF is a generalized Maxwellian VDF in that as κ approaches infinity, the distribution approaches Maxwellian. A number of normalized variations of the Lorentzian distribution are given in Figure 2, which demonstrates that smaller values of κ represent VDFs with more extended high-energy tails.

[19] Using the new STIM results, this study explores the scope of possible ionospheric contributions to the ion and electron populations in Saturn's plasmasphere by using the model of *Pierrard and Lemaire* [1996] for a Lorentzian velocity distribution at the exobase. Lorentzian distribution functions have an additional free parameter κ that determines the slope of the energy spectrum of the suprathermal particles in the tail of the distribution. Typical values for κ in space plasmas are 2–7 [*Scudder*, 1992; *Pierrard and Lemaire*, 1996]. The ideal assumption is made here that trapped particles do not contribute significantly to the plasmaspheric distributions. This is identical to the assumption that trapped particles are removed from a flux tube as quickly as they are brought into trapped orbit by collisional deflections. Such an approximation seems valid at Saturn because of the large extent of plasmaspheric flux tubes, the relatively small electron densities measured at Saturn, and, perhaps most importantly, the presence of the ring system, which can scatter or absorb incident particles.

[20] The *Pierrard and Lemaire* [1996] formalism contains a substantial set of equations covering over two pages of text. Thus, in order to conserve space the equations governing the distributions of plasma densities, temperatures, and pressures are not reproduced here, and instead, the reader is referred to the original derivations given by *Pierrard and Lemaire* [1996, and references therein].

3. Results

3.1. Global Plasmaspheric Distributions

[21] In order to isolate the effects of Maxwellian and Lorentzian VDFs on solar-derived plasmaspheric electron densities at Saturn the free parameters are minimized. A κ of 2 is chosen to represent the upper boundary of possible Lorentzian distributions. Lower κ indexes seem unlikely at Saturn, at least for low latitudes, because the radiation environment is mild compared to regions where $\kappa < 2$, such as the solar corona. Higher values of κ deplete the high-energy tail of the distribution and make it more Maxwellian; thus the electron density distributions derived herein using Lorentzian (κ = 2) and Maxwellian ($\kappa = \infty$) VDFs represent upper and lower boundaries for Saturn's plasmasphere. Plasma densities are generated first for equi-

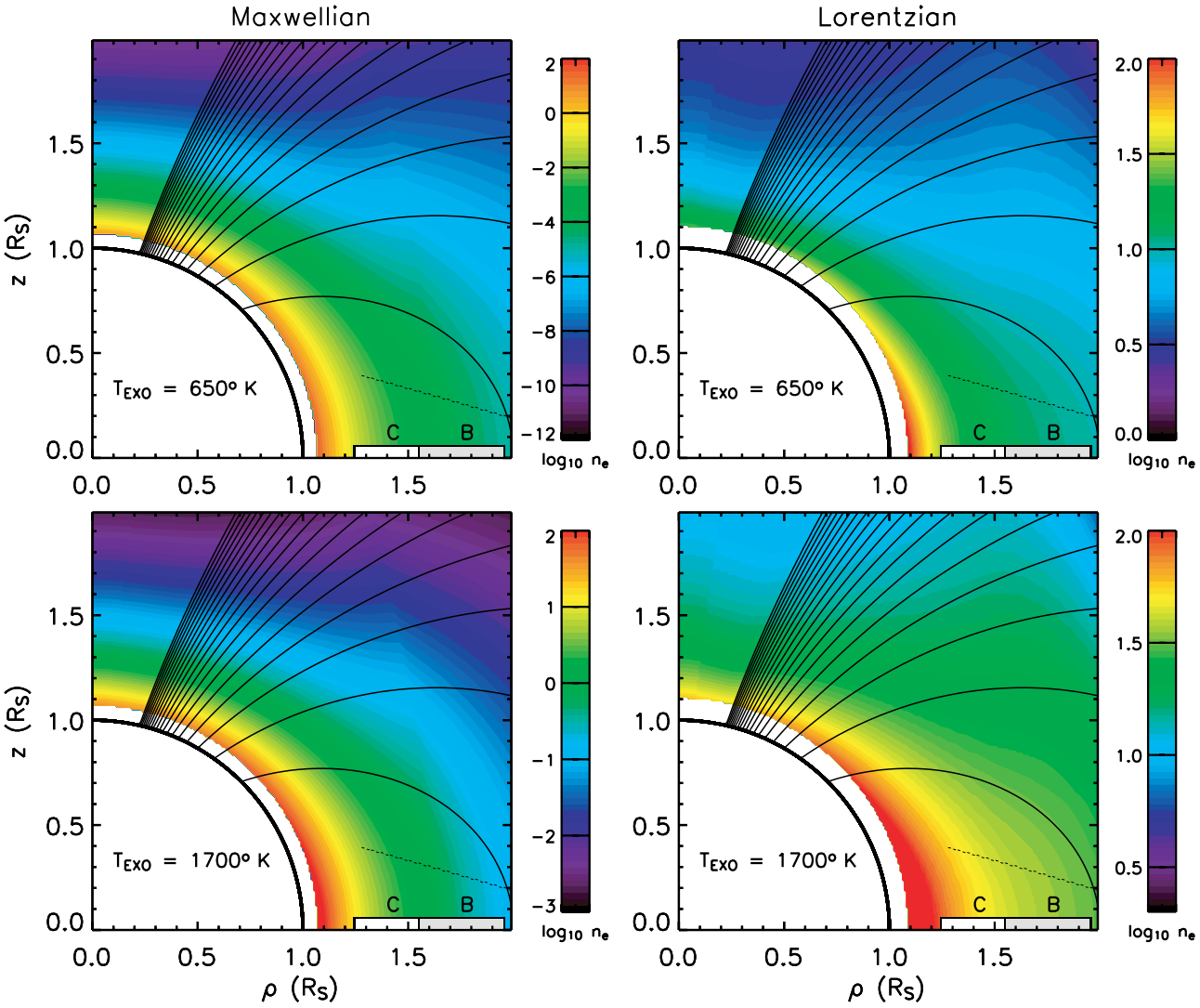

Figure 3. Plasmaspheric ion densities at Saturn during equinox for two velocity distributions, Lorentzian ($\kappa = 2$) and Maxwellian ($\kappa = \infty$), and two different temperatures at the plasma exobase, 650 and 1700 K. The densities at the exobase (Figure 1b) are extended into the plasmasphere using the *Pierrard and Lemaire* [1996] formulation. Note the different color bars for the various panels. Dipole field lines for $L = 1, 2, 3, \ldots, 20$ are plotted over the contours in each panel. The slight discontinuity at around $r = 1.6\ R_S$ is an artifact of the different calculation regimes within and without the Roche surface. Other discontinuities are results of the latitude resolution of the plasma exobase densities (1°, Figure 1b). The dotted lines mark the path of closest approach of the Cassini spacecraft during orbit insertion on 1 July 2004. Positions of Saturn's B and C rings are given along the x axis.

nox conditions in order to isolate and to identify the effects of different VDFs. Finally, in order to compare with Cassini measurements of plasma density a range of predicted plasma densities for southern summer (the geometry of the Cassini orbit insertion) are calculated using solar fluxes for July 2004. The temperature range of the plasma at the examined exobase is 650–1700 K, based on radio occultation observations, as discussed in section 1.2. Finally, adopted exospheric temperatures are assumed to be constant with latitude as a first approximation.

[22] Figure 3 displays model calculations for the two extreme velocity distributions for solar maximum conditions during equinox. Note the different color bars for each panel. Two different temperatures are used to represent the range of observed plasma temperatures at the plasma exobase: 650 and 1700 K. White areas above the surface of Saturn represent the ionosphere, and hence densities are not displayed. The plasmasphere is greatly extended in the $T_{exo} = 1700$ K case, compared with the $T_{exo} = 650$ K case. Additionally, it is clear that the electron density falls off much more rapidly for the Maxwellian VDF ($\kappa = \infty$) than for the Lorentzian VDF ($\kappa = 2$), an effect of the high-energy tail of the Lorentzian VDF. For example, in the $T_{exo} = 650$ K case the Maxwellian distribution leads to a reduction in electron density of nearly 14 orders of magnitude in the polar direction, while the Lorentzian distribution ($\kappa = 2$) leads to a reduction of fewer than 2 orders of magnitude. Calculations using solar minimum conditions demonstrate

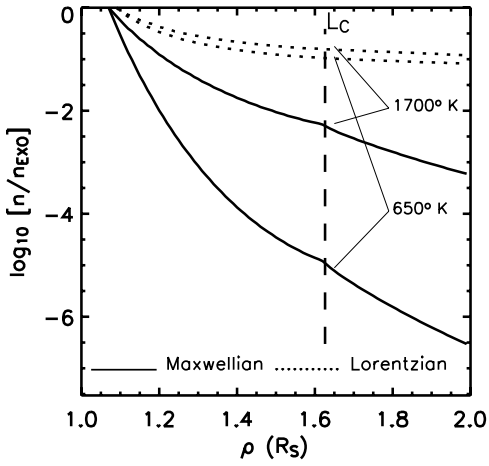

Figure 4. Equatorial plasmaspheric ion densities at Saturn during equinox for both Maxwellian ($\kappa = \infty$) and Lorentzian ($\kappa = 2$) velocity distributions and for two different temperatures at the plasma exobase. The top (bottom) dotted and solid lines correspond to calculations made with an exospheric plasma temperature of 1700 K (650 K) for Lorentzian and Maxwellian velocity distributions, respectively. The dashed line represents the critical radius where gravitational and centrifugal forces are balanced (equation (1)).

similar behavior to that shown in Figure 3, although the electron densities are about a factor of 2 smaller.

[23] In order to quantify the range of differences between plasmaspheric calculations coupled to a self-consistent thermosphere-ionosphere from below, the equatorial electron densities from Figure 3 are given in Figure 4. The predicted equatorial plasma densities lie within the region bounded by the top dotted line and the bottom solid line. This region defines the allowable equatorial plasma densities in Saturn's plasmasphere during equinox on the basis of a few simple assumptions: (1) The bulk of Saturn's middle- and low-latitude ionosphere is produced by solar insolation (as described by *Moore et al.* [2004], *Moses and Bass* [2000], *Majeed and McConnell* [1991], and others) and (2) the effects of Saturn's rings on equatorial plasmaspheric distributions within 2 R_S are minimal. The first assumption is quite safe, while the second seems unlikely, as discussed in section 3.3. In the meantime, it is useful to note that improved knowledge of either plasma temperature or velocity distribution at the exobase will serve to further constrain the region of predicted plasma densities given above, as $\kappa = 2$ is a lower boundary, and Lorentzian distributions with larger κ will tend toward Maxwellian distributions.

3.2. Flux Tube Content

[24] An added benefit of a global ionosphere-plasmasphere model is that the total flux tube electron content can be studied at Saturn. In the terrestrial case the plasmaspheric contribution to the flux tube content exceeds the contribution from the ionosphere by 1 or more orders of magnitude, and so plasma is shifted back and forth between the two domains as part of the diurnal maintenance of the ionosphere. Saturn's plasmasphere is much less dense, and despite the relatively large size of the flux tubes, its contribution to the total flux tube content is smaller than in the terrestrial case. Calculations for total flux tube electron content at Saturn during equinox are given in Figure 5, where the ionospheric contribution is calculated between 1000 and 4000 km and the plasmaspheric contribution comes from the plasma beginning at 4000 km

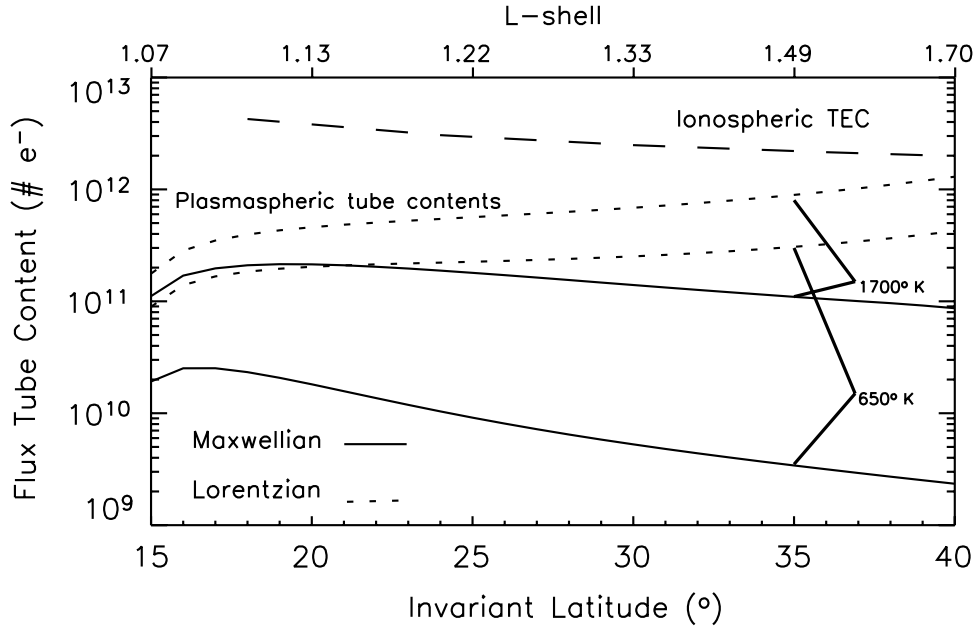

Figure 5. Total electron content for flux tubes with an area of 1 cm^2 at 4000 km altitude. Dotted and solid lines represent contributions from the plasmasphere for Lorentzian ($\kappa = 2$) and Maxwellian ($\kappa = \infty$) distributions, respectively, while the dashed line gives the ionospheric total electron content (TEC) for the same latitudes. Calculations are for solar maximum during equinox.

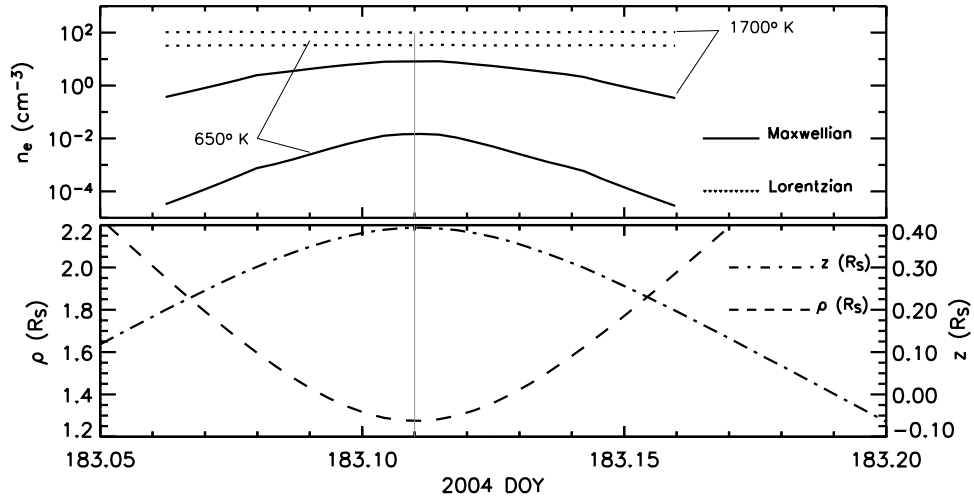

Figure 6. (top) Modeled plasmaspheric densities for Cassini's closest approach during orbit insertion on 1 July 2004 (day of year (DOY) is 183). (bottom) Plot of ρ and z, which are Cassini's equatorial radius and height above the equatorial plane, respectively. These calculations are based on a self-consistent thermosphere-ionosphere that determines the parameters of the plasma exobase. The plasma densities are then extended in altitude using the *Pierrard and Lemaire* [1996] formulation for Lorentzian ($\kappa = 2$) and Maxwellian ($\kappa = \infty$) distributions. The absolute boundaries of the prediction are the 650 K Maxwellian curve and the 1700 K Lorentzian curve, although further knowledge of either plasma exobase temperatures or temperature distributions would tighten these boundaries considerably. The vertical line marks the point of closest approach, which occurred at ~0240 UT.

altitude and continuing along the flux tube into the equatorial plane. A flux tube area of 1 cm^2 is assumed at 4000 km, and the flux tube area increases with distance along the field line to a maximum at the equatorial plane. From Figure 5 it is clear that the reservoir of thermal plasma in the innermost magnetosphere (L = 1.1–1.7), derived from purely ionospheric sources, cannot be a major driver of plasmasphere-ionosphere transport or of interhemispheric transport within the plasmasphere, as the plasmaspheric flux tube content is significantly less than the ionospheric content. This might not be the case at large L values for solstice conditions.

3.3. Previous Studies: Ring Effects

[25] There are four classes of exospheric particles of ionospheric origin [*Lemaire and Scherer*, 1971]. Escaping particles are those with large enough kinetic energy and small enough pitch angle to reach (and to cross) the equatorial plane. In the polar exosphere these particles can escape along open field lines and form a polar wind [*Schunk and Nagy*, 2000; *Banks and Kockarts*, 1973]. Incoming particles are then those that have escaped from the conjugate ionosphere. Ballistic particles possess either too small a kinetic energy or too large a pitch angle to reach the equatorial plane and are reflected magnetically back to the exobase within the same hemisphere. Trapped particles represent particles whose mirror points are located above the ion exobase. When all four classes of particles are in thermal equilibrium with each other, the pitch angle distribution is isotropic everywhere along the flux tubes. For partially or totally depleted populations of trapped particles (the assumption used here) the VDF is symmetric with respect to the parallel component of particle velocities, and there is no net flow along field lines.

[26] The plasma and neutrals from Saturn's rings can affect these cold, ionospheric distributions of plasma by acting as an absorber or scatterer [*Luhmann and Walker*, 1980], by acting as an active plasma source because of sputtering from meteors [*Ip*, 1984b], or by inhibiting plasma flow in flux tubes passing through the outer B ring and A ring due to ambipolar electric fields set up by warm ring plasma trapped in the equatorial plane by centrifugal force [*Wilson and Waite*, 1989].

[27] *Wilson and Waite* [1989] showed that the density of a Maxwellian distribution of ionospheric H^+ plasma with a temperature of 0.1 eV (~1160 K) located at 2500 km altitude would decrease by 2–3 orders of magnitude from the exobase to 1.5 R_S in the equatorial plane. Wilson and Waite used a two-stream semikinetic plasma model [*Li et al.*, 1988] to find the steady state flow between H^+ from below and O^+ from above along diverging magnetic flux tubes. By setting the lower boundary as the altitude of the observed electron density peak and the upper boundary as the ring plane and by making some estimates of source functions at each boundary, they conclude that H^+ would be the dominant ion in the inner ring system ($\geq$1.0 cm^{-3}), while O^+ would dominate the outer rings ($\leq$50 cm^{-3}). The high-temperature Maxwellian calculation in this study agrees well in terms of rate of decrease in density with radius (Figure 4). An important point can be drawn from this comparison: It is clear that the choice of altitude of the exobase has little noticeable effect on the final plasma density distribution at these scales, as Wilson and Waite used 2500 km, while ~4000 km was used here.

[28] *Luhmann and Walker* [1981] used the model developed by *Lemaire* [1976] to describe a plasma with a Maxwellian VDF in a rotating dipole field; they used an exobase at 6000 km with an electron density of 10^5 cm^{-3}.

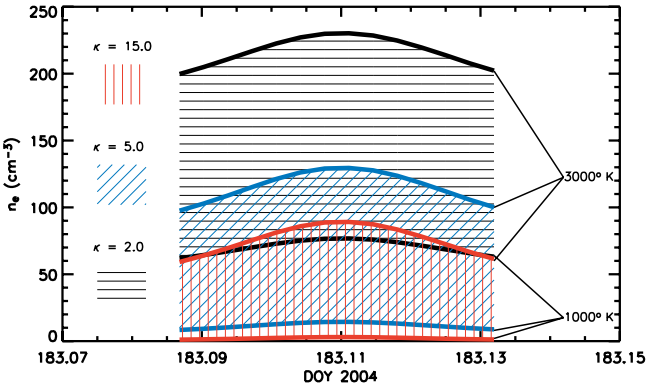

Figure 7. Modeled plasmaspheric electron densities along the path of Cassini's orbital insertion. The three domains represent calculations for three different values of κ, with temperatures ranging from 1000 to 3000 K in each case. There is a wide range of κ values and temperatures that would lead to predictions of ~70–100 cm^{-3} for plasma densities at Cassini's closest approach (DOY of 183.11, r of 1.3 R_S, and L shell of ~1.4).

They found that assuming that the rings completely remove all of the trapped ionospheric plasma, a temperature of 8000 K is required for the Lemaire formulation to adequately reproduce Pioneer 11 Saturn radio occultation data. This implies that either the ionospheric plasma is non-Maxwellian (i.e., Lorentzian) or there is significant plasma contribution from the rings or that some combination of the two holds true.

[29] While it is gratifying to see a general agreement with previous studies and to understand how different boundary conditions and VDF assumptions account for differences, this work strives to extend those studies by identifying the range of allowable plasmaspheric densities due to ionospheric plasma, and it does so by using a self-consistent thermosphere-ionosphere to define the plasma exobase parameters. As discussed in section 3.1, the assumption has been made in this study that the rings help to remove trapped particles from the density distributions. If this assumption is false, density distributions due to ionospheric plasma could be increased by up to a factor of 2 [*Luhmann and Walker*, 1981]. *Ip* [1984b] estimates the density of photoionized hydrogen near the rings to be ~10^{-3} cm^{-3}. In addition, there are larger estimates for nonhydrogen ring-derived plasma due to meteoroid impact. *Morfill et al.* [1983] calculate a ring plane density of 2–20 cm^{-3}, assuming H_2O^+ ions with a temperature of 2 eV. *Wilson and Waite* [1989] find that ring-derived O^+ ions (<50 cm^{-3}) are dominant over H^+ ions of ionospheric origin in the outer ring plane. *Richardson and Jurac* [2004] self-consistently derive plasma densities of primarily H_2O^+ and OH^+ ions using Voyager plasma and H observations and Hubble Space Telescope OH measurements as constraints. They find a peak electron density of ~100 el cm^{-3} centered near 4 R_S. Thus, as calculations in this work do not account for ring-derived plasma, the predictions made for radii greater than ~1.6 R_S (the critical radius, r_c) are a lower limit on plasmaspheric densities. Calculations within 1.6 R_S should still be accurate, however, as previous studies confirm that this is a region dominated by ionospheric H^+ plasma.

3.4. Comparisons With Observations

[30] During orbit insertion on 1 July 2004 the Cassini spacecraft passed through the inner plasmasphere of Saturn with the point of closest approach at a radius of 1.3 R_S. Instruments aboard Cassini, such as the Cassini Plasma Spectrometer, the Ion and Neutral Mass Spectrometer, and the Radio and Plasma Wave Science instrument (RPWS), will report observations of plasma parameters that can be directly compared to the predictions made here.

[31] The path of Cassini during orbit insertion is given in Figure 6 as height above the ring plane and equatorial radius as a function of time. The extremes of the inner plasmaspheric distribution (i.e., hot and cold and Maxwellian and Lorentzian) are calculated for southern summer and are given as a function of time in Figure 6 (first panel). The resulting range of densities during closest approach is 10^{-2}–10^{2} el cm^{-3}. Previous measurements of electron density in Saturn's plasmasphere by the Voyager 1 and 2 spacecraft show a heavy ion species (usually designated O^+) near the rings of order 10^2 cm^{-3} and an H^+ "cloud" above the rings of order 10^1 cm^{-3} [*Lazarus and McNutt*, 1983]. The Voyager measurements did not go within ~3 R_S, however, and were constrained by a low-energy threshold of 10 eV, thereby not accounting for the colder ion populations of this study.

[32] Preliminary results from measurements made by the Cassini instruments are just starting to appear in the literature as this report goes to press. Unfortunately, at closest approach the spacecraft engine firings for orbit insertion precluded, in many cases, the in situ data sets at 1.3 R_S most crucial to this study. In the only published results available at this time the RPWS instrument reported highly variable and depleted plasma densities within 2 R_S [*Gurnett et al.*, 2005], broadly consistent with the range of possibilities shown in Figures 4 and 6. With the full set of Cassini results still to come, the rest of this section is devoted to a set of calculations focused on the region of closest approach.

[33] It seems likely that the VDF at Saturn's plasma exobase is non-Maxwellian and relatively warm: (1) The plasma exobase is located at a higher altitude than the neutral exobase, (2) it is immersed in superthermal radiation, and (3) plasma temperatures for other gas giants are significantly higher than the 650 K minimum explored here. In other words, while there is no hard evidence to discount the entire range of electron density predictions given in Figure 6, it is probable that the plasmaspheric densities at Saturn lie within the upper half of the predictions. To account for the lack of knowledge of plasma temperature and VDF at the plasma exobase, electron densities are calculated for a more inclusive range of κ and temperatures in Figure 7, in which three domains are derived for three different values of κ. Each domain gives electron density calculations along the path of Cassini's orbital insertion for plasma temperatures at the exobase from 1000 to 3000 K. Where the three domains overlap, there is a wide range of temperatures and κ that would predict an electron density of ~100 cm^{-3} at L = 1.3. *Richardson and Jurac* [2004] predict electron densities of ~30 cm^{-3} near 2 R_S; however, their

plasma is derived from Enceladus and Saturn's E ring and is dominated by H_2O^+ and OH^+ ions. Therefore it seems reasonable to conclude that the purely ionospheric contribution to Saturn's inner plasmasphere could be an important component, at least out to 2 R_S.

4. Summary

[34] A method of coupling the Saturn thermosphere-ionosphere model (STIM) to a plasmaspheric model has been developed that takes full advantage of the global aspects of STIM. Saturn's plasmasphere is more complicated than Earth's in that there are more sources of plasma (sputtering from rings and moons in addition to the ionospheric outflow) and the full range of plasma ring interactions is unknown. Additionally, Saturn's plasmasphere is much less dense, and its relative contribution to the total flux tube content is significantly smaller than in the terrestrial case. Therefore it is unlikely that a model needs to take into account plasma flux from the plasmasphere into the ionosphere unless as part of a general asymmetry.

[35] The model results presented here give insight into what sort of plasma is to be expected in Saturn's inner plasmasphere. This insight comes as a result of identifying the important free parameters that drive the plasmaspheric density distributions, namely, plasma temperature and velocity distribution at the exobase. Instruments aboard the Cassini spacecraft are able to determine plasma temperatures and densities, therefore revealing the velocity distribution at the exobase. For instance, if a density of 10 el cm^{-3} were observed at closest approach, this analysis would lead to the conclusion that Saturn's inner plasmasphere is populated by a high-temperature Maxwellian VDF, a low-temperature Lorentzian VDF (with $\kappa > 2$), or something in between. Concurrent temperature information would constrain the velocity distribution further.

[36] It is certain that there are many complicated processes occurring in Saturn's plasmasphere and that this treatment has simplified many of them. However, previous studies of additional plasma generating processes support the assertion that within $\sim$1.6 R_S, Saturn's plasmasphere is dominated by ions (primarily H^+) and electrons of ionospheric origin. By isolating and determining one of the two main sources of plasma in Saturn's ring plane (i.e., ionospheric plasma) it becomes easier to quantify the contributions from other ring-derived sources of plasma and possible changes in the ionospheric plasma via ion-neutral interactions near the rings.

[37] **Acknowledgments.** SOLAR2000 Research Grade historical irradiances are provided courtesy of W. Kent Tobiska and http://www.spacewx.com. These historical irradiances have been developed with funding from the NASA UARS, TIMED, and SOHO missions. Support for this work was provided by a grant from the NASA Planetary Atmospheres Program. L.M. acknowledges support from a NASA Graduate Student Research Program fellowship.

[38] Arthur Richmond thanks Andrew F. Nagy and another reviewer for their assistance in evaluating this paper.

References

Angerami, J. J., and J. O. Thomas (1964), Studies of planetary atmospheres: 1. The distribution of electrons and ions in the Earth's exosphere, *J. Geophys. Res.*, *69*, 4537–4560.

Atreya, S. K., J. H. Waite, T. M. Donahue, A. F. Nagy, and J. C. McConnell (1984), Theory, measurements and models of the upper atmosphere and ionosphere of Saturn, in *Saturn*, edited by T. Gehrels and M. S. Matthews, pp. 239–277, Univ. of Ariz. Press, Tucson.

Banks, P. M., and G. Kockarts (1973), *Aeronomy*, Elsevier, New York.

Brown, M. E. (1994), Observation of mass loading in the Io plasma torus, *Geophys. Res. Lett.*, *21*, 847–850.

Burch, J. L. (2003), The first two years of IMAGE, *Space Sci. Rev.*, *109*, 1–24.

Carpenter, D. L., and C. G. Park (1973), On what ionospheric workers should know about the plasmapause-plasmasphere, *Rev. Geophys.*, *11*, 133–154.

Dessler, A. J. (1980), Mass-injection rate from Io into the Io plasma torus, *Icarus*, *44*, 291–295.

Gladstone, G. R., R. V. Yelle, and R. Majeed (2002), Solar system upper atmospheres: Photochemistry, energetics and dynamics, in *Atmospheres in the Solar System: Comparative Aeronomy*, *Geophys. Monogr. Ser.*, vol. 130, edited by M. Mendillo, A. Nagy, and J. G. Waite, pp. 23–37, AGU, Washington, D. C.

Gurnett, D. A., et al. (2005), Radio and plasma wave observations at Saturn from Cassini's approach and first orbit, *Science*, *307*, 1255–1259.

Hartle, R. E. (1969), Ion-exospheres with variable conditions at the baropause, *Phys. Fluids*, *12*(2), 455–462.

Hartle, R. E. (1971), Model for rotating and nonuniform planetary exospheres, *Phys. Fluids*, *14*(12), 2592–2598.

Hasegawa, A., K. Mima, and M. Duong-Van (1985), Plasma distribution function in a superthermal radiation field, *Phys. Rev. Lett.*, *14*, 2609–2610.

Ip, W.-H. (1983), On plasma transport in the vicinity of the rings of Saturn: A siphon flow mechanism, *J. Geophys. Res.*, *88*, 819–822.

Ip, W.-H. (1984a), On the equatorial confinement of thermal plasma generated in the vicinity of the rings of Saturn, *J. Geophys. Res.*, *89*, 395–398.

Ip, W.-H. (1984b), Electrostatic charging of the rings of Saturn: A parameter study, *J. Geophys. Res.*, *89*, 8843–8849.

Kim, Y. H., and S. Son (2000), The effects of planetary rotation on the exospheric density distributions of the Earth and Mars, *J. Korean Astron. Soc.*, *33*, 127–135.

Lazarus, A. J., and R. L. McNutt Jr. (1983), Low-energy plasma ion observations in Saturn's magnetosphere, *J. Geophys. Res.*, *88*, 8831–8846.

Lemaire, J. (1976), Rotating ion-exospheres, *Planet. Space Sci.*, *24*, 975–985.

Lemaire, J., and M. Scherer (1971), Simple model for an ion-exosphere in an open magnetic field, *Phys. Fluids*, *14*(8), 1683–1694.

Lemaire, J., and M. Scherer (1974), Exospheric models of the topside ionosphere, *Space Sci. Rev.*, *15*, 591–640.

Li, P., G. R. Wilson, J. L. Horwitz, and T. E. Moore (1988), Effect of mid-altitude ion heating on ion outflow at polar latitudes, *J. Geophys. Res.*, *93*, 9753–9763.

Luhmann, J. G., and R. J. Walker (1980), Some possible effects of Jupiter's rings on the Jovian inner plasmasphere, *Icarus*, *44*, 361–366.

Luhmann, J. G., and R. J. Walker (1981), Model exospheres of the ringed planets, *Geophys. Res. Lett.*, *8*, 107–110.

Majeed, T., and J. C. McConnell (1991), The upper ionospheres of Jupiter and Saturn, *Planet. Space Sci.*, *39*, 1715–1732.

Majeed, T., and J. C. McConnell (1996), Voyager electron density measurements on Saturn: Analysis with a time dependent ionospheric model, *J. Geophys. Res.*, *101*, 7589–7598.

Maksimovic, M., V. Pierrard, and P. Riley (1997), Ulysses electron distributions fitted with kappa functions, *Geophys. Res. Lett.*, *24*, 1151–1154.

Meyer-Vernet, N. (2001), Large scale structure of planetary environments: The importance of not being Maxwellian, *Planet. Space Sci.*, *49*, 247–260.

Moore, L. E., M. Mendillo, I. C. F. Müller-Wodarg, and D. L. Murr (2004), Modeling of global variations and ring shadowing in Saturn's ionosphere, *Icarus*, *172*, 503–520.

Morfill, G. E., H. Fechtig, E. Grün, and C. K. Goertz (1983), Some consequences of meteoroid impacts on Saturn's rings, *Icarus*, *55*, 439–447.

Moses, J. I., and S. F. Bass (2000), The effects of external material on the chemistry and structure of Saturn's ionosphere, *J. Geophys. Res.*, *105*, 7013–7052.

Nagy, A. F., A. R. Barakat, and R. W. Schunk (1986), Is Jupiter's ionosphere a significant plasma source for its magnetosphere?, *J. Geophys. Res.*, *91*, 351–354.

Pierrard, V., and J. Lemaire (1996), Lorentzian ion exosphere model, *J. Geophys. Res.*, *101*, 7923–7934, (Correction, *J. Geophys. Res., 103,* 4117–4118, 1998.).

Richardson, J. D., and S. Jurac (2004), A self-consistent model of plasma and neutrals at Saturn: The ion tori, *Geophys. Res. Lett.*, *31*, L24803, doi:10.1029/2004GL020959.

Schunk, R. W., and A. F. Nagy (2000), *Ionospheres: Physics, Plasma Physics, and Chemistry*, Cambridge Univ. Press, New York.

Scudder, J. D. (1992), On the causes of temperature change in inhomogeneous low-density astrophysical plasmas, *Astrophys. J.*, *398*, 299–318.

Sittler, E. C., Jr., K. W. Ogilvie, and J. D. Scudder (1983), Survey of low-energy plasma electrons in Saturn's magnetosphere: Voyagers 1 and 2, *J. Geophys. Res.*, *88*, 8847–8870.

Smith, G. R., D. E. Shemansky, J. B. Holberg, A. L. Broadfoot, B. R. Sandel, and J. C. McConnell (1983), Saturn's upper atmosphere from the Voyager-2 EUV solar and stellar occultations, *J. Geophys. Res.*, *88*, 8667–8678.

Spitzer, L., Jr. (1949), The terrestrial atmosphere above 300 km, in *The Atmospheres of the Earth and Planets*, edited by G. P. Kuiper, pp. 213–249, Univ. of Chicago Press, Chicago, Ill.

Tobiska, W. K., T. Woods, F. Eparvier, R. Viereck, L. Floyd, D. Bouwer, G. Rottman, and O. R. White (2000), The SOLAR2000 empirical solar irradiance model and forecast tool, *J. Atmos. Sol. Terr. Phys.*, *62*, 1233–1250.

Wilson, G. R., and J. H. Waite Jr. (1989), Kinetic modeling of the Saturn ring-ionosphere plasma environment, *J. Geophys. Res.*, *94*, 17,287–17,298.

Yelle, R. V., and S. Miller (2004), Jupiter's thermosphere and ionosphere, in *Jupiter: Planet, Satellites and Magnetosphere*, edited by F. Bagenal, W. McKinnon, and T. Dowling, pp. 185–218, Cambridge Univ. Press, New York.

M. Mendillo and L. Moore, Center for Space Physics, Boston University, 725 Commonwealth Avenue, Boston, MA 02215, USA. (moore@bu.edu)